J Mol Model (2008) 14:237–247
DOI 10.1007/s00894-007-0266-8

ORIGINAL PAPER

# Theoretical investigation of direct amination of β-ketoesters catalyzed by copper(II)-bisoxazoline(BOX)

**Youqing Yu · Wei Shen · Jinsheng Zhang · Rongxing He · Ming Li**

Received: 17 September 2007 / Accepted: 14 December 2007 / Published online: 29 January 2008


**Abstract** The mechanism of the direct amination of β-keto esters catalyzed by copper(II)-bisoxazoline has been studied by means of density functional theory of B3LYP method. The computational results support the present mechanism, which involves (i) the generation of the enol from β-keto esters, which coordinates to copper(II)-bisoxazoline. The coordination step appears to be fast, exothermic, and irreversible. (ii) The formation of the σ(N-C) bond via a six-membered ring transition state after azo dicarboxylate coordination with the chiral catalyst. This step is chirality-control step. (iii) Intramolecular hydrogen migration generates a catalyst-product complex, which can finally yield product. The hydrogen shift is the rate-determining step, which affords the experimentally observed (R)-product. The stereochemical predictions have been rationalized in terms of steric repulsions, showing good agreement with experimental data.

**Keywords** Copper(II)-catalyzed · DFT · Direct amination · Reaction mechanism

## Introduction

Optically active α-amino acid derivative are fundamental constituents of numerous natural products and of other highly valuable compounds for our daily life. As a result, great efforts have been made to develop efficient diastereo- and enantio-selective methods for the synthesis of α-amino acid derivatives [1–6]. However, the development of stereoselective transformations for the synthesis of optically active non-nature α-amino acid derivatives from simple and readily available starting compounds in the presence of a chiral catalyst is an ongoing challenge for chemists.

The synthesis of optically active α-amino acid derivatives by a catalytic, enantioselective, direct C-N bond forming reaction is probably among the simplest procedures for the formation of an asymmetric carbon center attached to a nitrogen atom [7–14]. Recently, Jørgensen and co-workers present the first direct α-amination of α-substituted β-ketesters 1 catalyzed by a chiral copper(II)-bisoxazoline (BOX) complex with azodicarboxylates 2 as the nitrogen fragment source [15, 16] (see Scheme 1). The reaction are catalyzed by chiral copper(II)-bisoxazoline (BOX) to give the products in high yields and excellent enantiomeric excesses. This new reaction gives access to β-hydroxy-α-amino acids such as oxazolindinone derivatives.

In particular, C2-symmetric bis(oxazoline) (BOX) ligands in the presence of copper salts have been used for numerous catalytic asymmetric reaction because of their efficiency, selectivity, and broad substrate tolerance [17–19]. Of these, the mechanism of Lewis acid-catalyzed direct α-amination reaction using bis(oxazoline) copper(II) complexes remains unclear and is the subject of this article.

A detailed understanding of the reaction mechanism is necessary to rationalize the observed stereoselectivity and enantioselectivity, and to design better catalysts with higher enantioselectivity. Mechanistic studies show that copper (II)-bisoxazoline (BOX) fragment is the active species in the catalytic process. The coordination of β-keto esters to the active species is believed to be the first step in the direct α-amination (see Scheme 2). IN1 through TS1, via 1,3

**Electronic supplementary material** The online version of this article (doi:10.1007/s00894-007-0266-8) contains supplementary material, which is available to authorized users.

Y. Yu · W. Shen · J. Zhang · R. He · M. Li (✉)
Department of Chemistry, Southwest University, Chongqing 400715, People's Republic of China
e-mail: liming@swu.edu.cn

**Scheme 1** Enantioselective direct α-amination of α-substituted β-keto esters with azodicarboxylates catalyzed by chiral copper(II)-bisoxazoline (BOX)

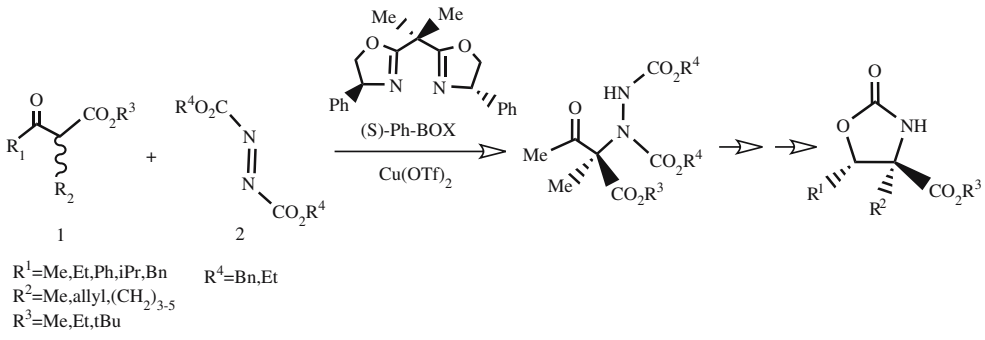


hydrogen shift, to form IN2. The keto-enol tautomerization of R1 and then coordinates with Cat to form IN2 is also discussed. The following azo dicarboxylate R2 coordinates with IN2 to give IN3. A subsequent N-C bond generation yield IN4, IN4 through hydrogen migrate step to give IN5. Finally, IN5 releases of product and regenerates Cat.

## Computational details

Molecular geometries of the model complexes were optimized at the B3LYP level of density functional theory [20, 21]. Frequency calculations at the same level of theory have also been performed to confirm that all stationary points were minima (no imaginary frequency) or transition states (one imaginary frequency). Calculations of intrinsic coordinates (IRC) [22] were also performed on transition states to confirm that such structures are indeed connecting two minima. The effective core potentials (ECPs) of Hay and Wadt with a double-ζ valance basis sets (Lanl2dz) [23–25] were used for Cu. The 6–31G* [26] basis set was chosen to describe C, H, O and N. All calculations were performed with Gaussian 03 software package [27]. The vibrational analysis and the natural bond orbital (NBO) analysis [28–36] were performed at the same computational level. In addition, the electron densities at the bond critical points (BCP) and the ring critical points (RCP) for selected bond of some species were calculated by employing the AIM2000 program package [37]. The completely topological analyses are performed for all the compounds to obtain detailed bonding character. The BCPs denoting as (3, -1), which represent saddle points in the electron densities between two atoms are examined for all the bonds. In the topological definition, a chemical bond is represented by the bond path. The gradient path links two neighboring nuclei along with maximal ρr in any neighboring lines. It was shown that ρ(r) and $\nabla^2_\rho(r)$ taken together can be employed to monitor the relative increase or decrease of charge accumulation.

In addition, solvent effects of dichloromethane were studied by performing self-consistent reaction field single-point calculations employing the polarizable continuum model (PCM) [38] approach on the B3LYP/6–31G* gas phase optimized geometry of each species at the same level. In this method, the solute is placed into a cavity within the solvent and the latter is modeled as a continuum of uniform dielectric constant. In this solvent model, the number of tessarae on each sphere was set to default value of 62. In order to yield more accurate energetic information, single-point (SP) calculations both of the gas-phase and solvent effects were carried out with the basis set of Lanl2dz adding one set of d-polarization function (exponent: 3.525) [39] for Cu and 6–311G(d,p) for other elements. Utilizing the Gibbs free energy including all electrostatic and non electrostatic terms, the reaction rate coefficients for key steps were computed by transition state theory.

Molecular orbital (MO) compositions and the overlap populations were calculated using the AOMix program

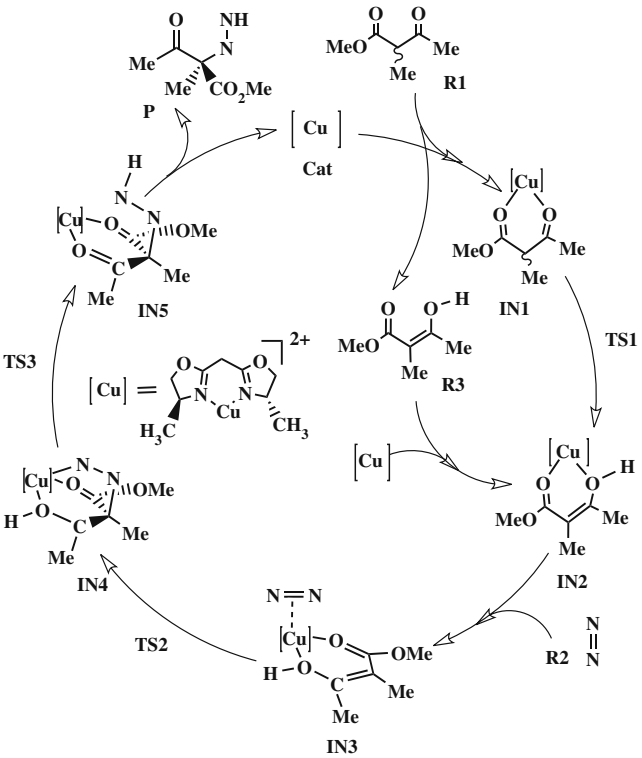


**Scheme 2** Catalytic cycle for copper-catalyzed direct amination reaction

**Table 1** Total Gibbs free energies G(×2625.5 kJ mol$^{-1}$), relative Gibbs free energies ΔG (kJ mol$^{-1}$), solvation energies $\Delta G^{sol}$ (kJ mol$^{-1}$), and frequencies(cm$^{-1}$) for selected compounds

| Species | Gas phase | | | In $CH_2Cl_2$ | | Frequencies | |
|---|---|---|---|---|---|---|---|
| | G | ZPE | [a]ΔG | G | $\Delta G^{sol}$ | $\nu_1$ | $\nu_2$ |
| R1–1 | −460.221199 | 0.156499 | – | −460.471177 | 3.0 | 11.7 | 51.9 |
| R1–2 | −460.219546 | 0.156820 | – | −460.470702 | 2.8 | 22.7 | 53.0 |
| R1–3 | −460.19494 | 0.156730 | – | −460.455818 | −0.09 | 41.2 | 86.0 |
| R2 | −566.300846 | 0.114421 | – | −566.538518 | 1.2 | 16.1 | 70.5 |
| Cat | −806.68394 | 0.231345 | – | −807.260402 | −137.7 | 36.2 | 41.2 |
| IN1-a | −1267.020685 | 0.392602 | −303.4 | −1267.826884 | −104.0 | 19.0 | 26.2 |
| TS1-a | −1266.912387 | 0.385260 | −19.0 | −1267.717074 | −103.5 | 2117.5i | 15.9 |
| IN2 | −1266.996868 | 0.391852 | −240.8 | −1267.808718 | −104.4 | 16.2 | 21.4 |
| IN3-a | −1833.299604 | 0.508037 | −5.0 | −1834.350702 | −84.1 | 15.0 | 15.4 |
| TS2-a | −1833.282375 | 0.508799 | 40.2 | −1834.342598 | −86.2 | 198.5i | 19.0 |
| IN4-a | −1833.301242 | 0.510493 | −9.2 | −1834.3641 | −86.7 | 15.9 | 27.1 |
| TS3-a | −1833.260944 | 0.505324 | 96.5 | −1834.320873 | −92.7 | 1408.8i | 14.7 |
| IN5-a | −1833.343318 | 0.512369 | −119.7 | −1834.40265 | −86.0 | 10.0 | 17.2 |
| P-a | −1026.537836 | 0.276720 | – | −1027.055246 | 5.7 | 26.6 | 46.6 |
| IN1-b | −1267.02204 | 0.392341 | −306.9 | −1267.826813 | −101.7 | 18.4 | 21.5 |
| TS1-b | −1266.914706 | 0.385114 | −25.1 | −1267.717596 | −102.5 | 2115.2i | 20.7 |
| IN2 | −1266.996868 | 0.391852 | −240.8 | −1267.808718 | −104.4 | 16.2 | 21.4 |
| IN3-b | −1833.293971 | 0.507933 | 9.8 | −1834.345285 | −85.5 | 11.7 | 14.8 |
| TS2-b | −1833.276224 | 0.508846 | 56.4 | −1834.336667 | −156.9 | 215.7i | 14.4 |
| IN4-b | −1833.296921 | 0.510665 | 2.1 | −1834.359049 | −86.7 | 14.9 | 28.5 |
| TS3-b | −1833.259223 | 0.504705 | 101.0 | −1834.32831 | −100.4 | 1429.1i | 13.8 |
| IN5-b | −1833.342417 | 0.512665 | −117.4 | −1834.405468 | −87.2 | 13.0 | 22.8 |
| P-b | −1026.540612 | 0.277097 | – | −1027.058760 | 5.8 | 27.8 | 49.0 |

a. the relative Gibbs free energies of IN1, TS1 and IN2 relative to R1–1+Cat, and the relative Gibbs free energies of IN3, TS2, IN4, TS3 and IN5 relative to R1–1+Cat+R2.

[40, 41]. The analysis of the MO compositions in term of occupied and unoccupied fragment molecular orbitals (OFOs and UFOs, respectively), the charge decomposition analysis (CDA), construction of orbital interaction diagrams analysis were performed using AOMix-CDA [42]. In AOMix program, the MOs of a molecular system can be expanded as linear combinations of the MOs of fragments.

## Results and discussion

Total Gibbs free energies (G) rectified with zero-point energies (ZPE), solvent effect energies $\Delta G^{sol}$, and the first two vibrational frequencies, $\nu_1$ and $\nu_2$, are summarized in Table 1. The electron densities (ρ(r)), the Laplacian $\left(\nabla^2_\rho(r)\right)$, and the Wiberg bond indexes (WBIs) [43] are listed in Table 2. In order to make the calculations more efficient and close to experimental condition, the model catalyst [$Cu^{II}${(S,S)-Me-BOX}] are used, and $R^1$, $R^2$, $R^3$, $R^4$ in the reactant 1 and 2 are replaced by methyl, respectively.

### Formation of IN2

The structures of the catalyst and reactants considered in this work are shown in Fig. 1. The catalyst (Cat) has a planar framework with a C2-symmetry. The coordination bond length of Cu-N is 1.916 Å. The C-N=N-C bond of azodicarboxylate (R2) also has a planar structure and the N=N bond length is 1.246 Å, as one would expect. On the

**Table 2** BCP properties and Wiberg bond indexes of the selected bonds in some structures

| Bond | Structure | $\varepsilon_{BCP}$ | $\nabla^2_{\rho(r)}$ | $\rho_{(r)}$ | WBI |
|---|---|---|---|---|---|
| Cu-O1 | Ts1-a | 0.069 | 0.34 | 0.050 | 0.10 |
| | Ts1-b | 0.079 | 0.36 | 0.054 | 0.11 |
| N3=N4 | In3-a | 0.13 | −0.98 | 0.469 | 1.90 |
| | In3-b | 0.13 | −1.12 | 0.478 | 1.91 |
| N3-N4 | Ts2-a | 0.11 | −0.84 | 0.412 | 1.43 |
| | Ts2-b | 0.10 | −0.84 | 0.409 | 1.41 |

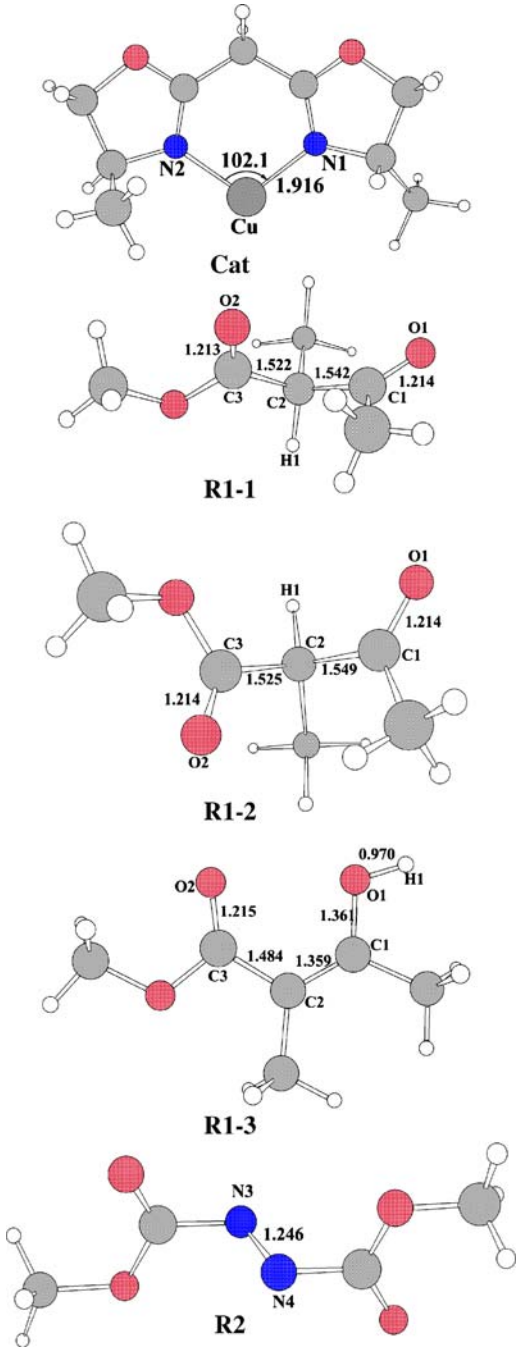


**Fig. 1** Structure of the catalyst (Cat), R1–1, R1–2, R1–3 and R2

other hand, for α-substituted β-keto ester (R1), both R (R1–2) and S (R1–1) conformations are depending on the relative position of the methyl and hydrogen. R1–1 is lower 4.3 kJ $mol^{-1}$ than R1–2 in energy.

*By 1,3 H shift to form IN2*

The structure of the catalyst-keto ester complexes (IN1) are shown in Fig. 2. The structure of IN1 presents a square-planar configuration, the dihedral angles between the O1-Cu-O2 plane and the bis(oxazoline) copper(II) plane are very similar in all the complexes. Two Cu-O1 bonds distance is 2.010 Å and 2.021 Å, respectively. The C1-O1 bond lengths are slightly lengthened due to coordinating to [CuII{(S,S)-Me-BOX}] (increase from 1.214 Å to 1.242 Å).

As can be seen from the Fig. 3, the released energy of R1 coordinate to Cat is 303.4 and 311.2 kJ $mol^{-1}$, respectively, which indicates this step to be fast, exothermic, and irreversible. However, the coordination transition state of R1 with Cat was not located at the theoretical levels used, which indicate that the coordination process is barrierless or, alternatively, has very low activation barrier (the scan curve along Cu-N3: see Fig. S1).

An intramolecular 1,3 hydrogen shift transition states (TS1) were located. Two conformations are possible for the TS1 and these depend on the orientation of the hydrogen (see TS1-a and TS1-b in Fig. 4). The H1 migration to O1 from C2 leads to a four-membered ring of C2-H1-O1-C1, a RCP of the ring is found (the electronic density is 0.084 for TS1-b). In TS1 the C2-H1 σ-bond and C1-O1 π-bond are partially broken, and the new O1-H1 σ-bond and C1-C2 π-bond are partially formed. It can be seen from AIM analysis, a BCP between O1-H1 in TS1-b is found (ρ(r)= 0.136), and for C1-C2 is 0.308. (see Fig. 5).

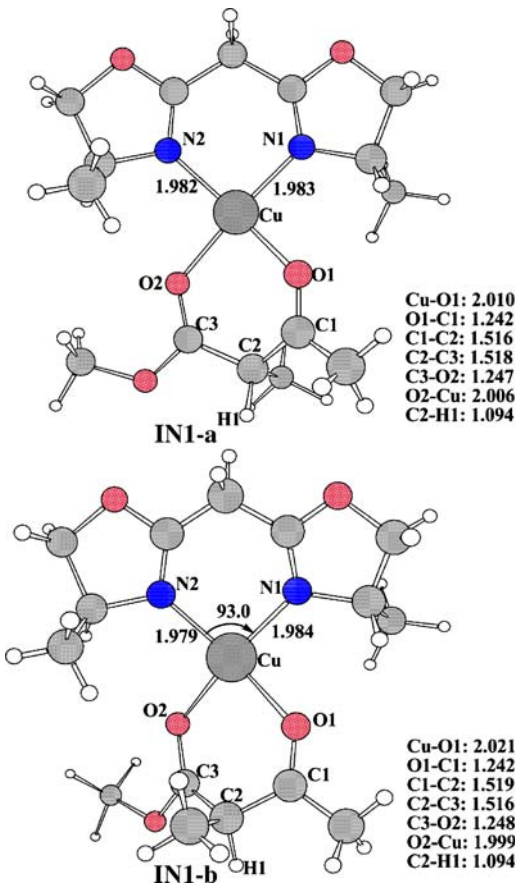


**Fig. 2** B3LYP optimized structures for IN1

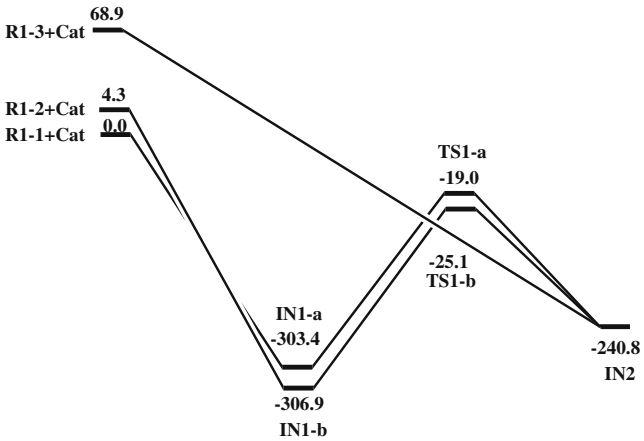


**Fig. 3** Energy profile calculated for the proposed IN2 formation. The relative energies are given in kJ mol$^{-1}$

From the structural viewpoint, TS1-a is very similar to TS1-b (see Fig. 4). They differ from the Cu-O1 bond distance. In TS1-a, there are clear steric interactions between the methyls of the 4-position of the oxazoline ring and the β-position of R1 (the distance is 2.377 Å). As in the case of TS1-a, this steric interaction leads to the Cu-O1 bond distance in TS1-a (2.110 Å) to be longer than that in TS1-b (2.084 Å). As show in Table 2, the electron density, ρ(Cu-O1), of TS1-b is slightly higher than that of TS1-a (0.054 versus 0.050). As steric interaction result, the forward reaction barrier of TS1-a is higher than that of TS1-b.

Examining the reaction energies, the barriers of 1,3 hydrogen migration via TS1-a and TS1-b are relatively high (284.4 and 281.8 kJ mol$^{-1}$, respectively) (Fig. 3). Although the coordination of R1–1 or R1–2 with Cat leave out a large of energy, considering the high barriers and the less stable intermediate IN2 (the relative energy of IN2 is 62.6 and 66.1 kJ mol$^{-1}$ higher than IN1-a and IN1-b), the formation of IN2 through 1,3 hydrogen of keto is difficult to occur.

*By 2-keto ester tautomery to form IN2*

The β-keto ester can exist mainly as two tautomeric forms in equilibrium (see Scheme 3); the β-keto ester form R1–1 and R1–2 is 68.9 and 64.6 kJ mol$^{-1}$ lesser in energy than isomer R1–3, respectively. With the inclusion of the solvent effect, this difference became 35.2 and 33.9 kJ mol$^{-1}$, respectively. Thus, this tautomeric form was assumed for the catalyzed process.

As shown in Fig. 3, R1–3 coordination with Cat is quite favored (the relative energy to IN2 is 309.7 kJ mol$^{-1}$). This reveals a good overlap between the LUMO of Cat and the

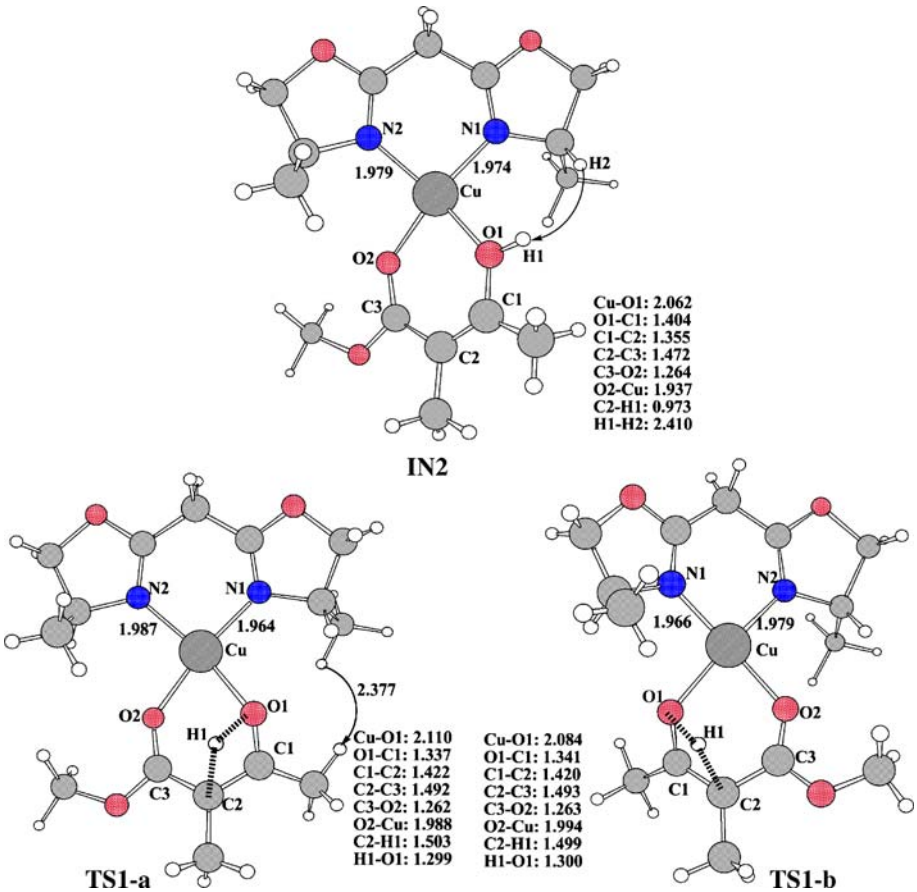


**Fig. 4** B3LYP optimized structures for TS1 and IN2

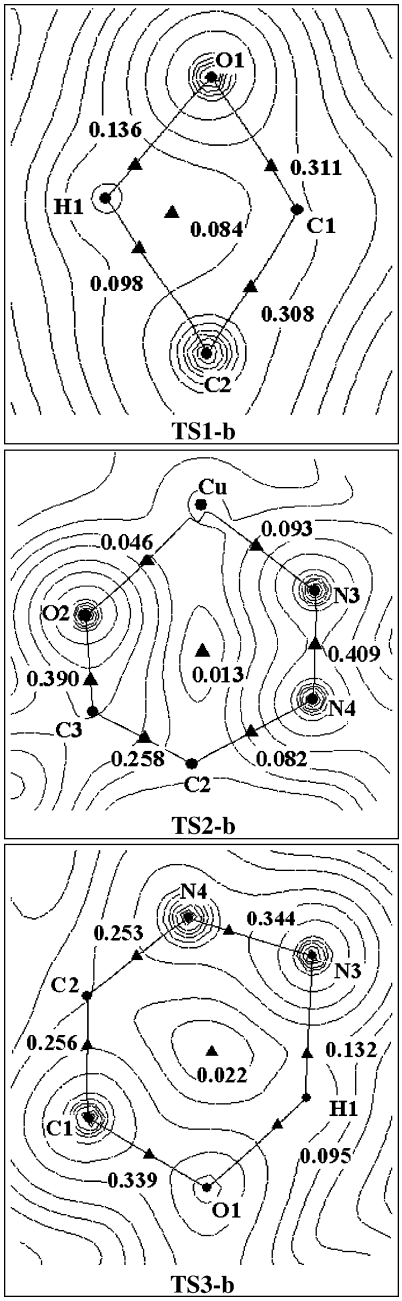


**Fig. 5** The two-dimensional electron density contours for all the transition states of pathway B (including electron densities of some selected BCPs and RCPs)

HOMO of the R1–3. Compared to the interaction between $HOMO_{Cat}$(-0.58eV) and $LUMO_{R1–3}$(-0.01eV), the contribution from the interaction between $HOMO_{R1–3}$(-0.22eV) and $LUMO_{Cat}$(-0.37eV) is large. As illustrated in Fig. 6, the R1–3 → Cat π-back-donation is almost exclusively produced by the interaction between the HOFO of R1–3 fragment ($HOFO_{R1–3}$) and the LUFO of the Cat fragment ($LUFO_{Cat}$). The LUMO-a of IN2 mainly comes from the contribution of $LUFO_{R1–3}$ (94.7%) and while the LUMO-b is a combination of 7% $HOFO_{R1–3}$, 9.7% $HOFO_{Cat}$, and 63.6% HOFO-$1_{Cat}$. The corresponding bonding orbital HOMO-a and HOMO-b is a combination of 88.6% $HOFO_{R1–3}$ and 87.8% $HOFO_{R1–3}$. These orbital contributions indicate the strong π-back-donation interaction between two fragments.

Thus, the favored coordination step make the R1 react with Cat by enol configuration, it is according with the observation of El-Dissouky, that the chiral bis (oxazoline)-copper(II) complex can promote the keto to enol tautomerization [44].

R1, by enol form R1–3, coordinate with Cat to form 17-electron complex IN2. Akin to R1–1 coordination with Cat, no transition state of R1–3 coordination with Cat was located. As shown in Fig. 4, the complex IN2 is likely a distorted square-planar geometry. O1-C1-C2-C3-O2 is nearly coplanar, and H1 is also in the plane. Owing to the steric interaction between the R1–3 ligand and the substituent in the 4-position of the oxazoline ring, the ligands plane twists (the angle between two planes defined by N1-Cu-N2 and O1-Cu-O2).

As reference [45] suggested, there is a relationship beween the enantioselectivity and the ligands plane twists in these systems catalyzed by metal coordination with C2-symmetric.

The Cu-N and Cu-O bond lengths are similar to those found in related complexes determined by X-ray analysis [46, 47]. The Cu coordination with O1 is less strong than that with O2 because of its longer distance (2.062 Å versus 1.937 Å).

## Formation of C-N σ-bond

Two possible conformations are located-depending on the orientation of R2 attack IN2. Figure 7 illustrates the calculated structures of IN3, as well as the structure parameters.

The structures of transition state connecting the energy minima corresponding to IN2→IN3 could not be located at the theoretical levels used, which indicates that the R2 attack process is barrierless, fast or has low barrier (see Fig. S2) just like the coordination between R1 and Cat.

Inspecting Fig. 7, it can be found the 4-coordination complex, IN2, affords IN3-a and IN3-b which are 5-coordination and 19-electron complexes. The big difference between Cu center with two N atoms (2.114 Å and 2.964 Å in IN3-a, 2.477 Å and 3.056 Å in IN3-b), it indicates that Cu center coordinate with only one N, and not with the N=N. It is in agreement with NBO analysis. As NBO analysis, the Wiberg bond index (which is use to examine

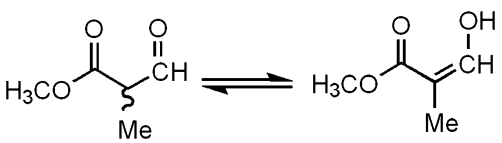


**Scheme 3** β-keto ester as two tautomeric forms

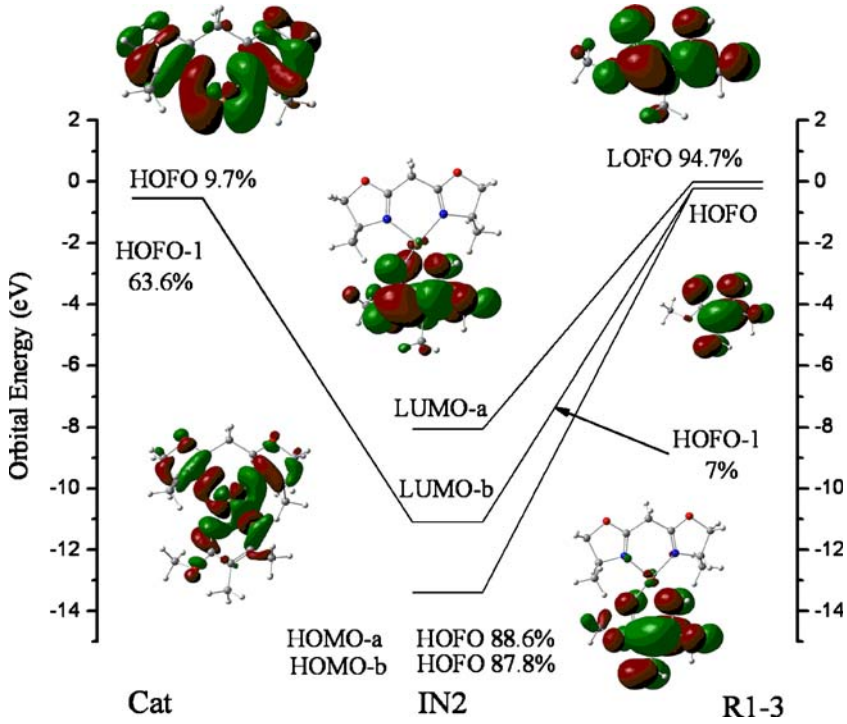


**Fig. 6** The orbital interaction diagram illustrating the coupling of Cat and R1–3 fragments in IN2 complex (the AOMix-CDA calculation, based on B3LYP/6–31g* results, MO of α and β electron replace with a and b, respectively). Because of the little deference in energy, some orbitals can not be divided clearly. The MO-FO pairs connected by lines if the corresponding FO contributions are greater than 5%

the component of π-bond) is 1.90 for N=N bond of IN3-a and 1.91 for IN3-b (see Table 2). It indicates the N=N bond includes obvious components of π-bond. In addition, the NBO charge of Cu, N3 and N4 is 1.32, -0.30 and -0.09 in IN3-a, and 1.37, -0.30 and -0.18 in IN3-b, respectively. These exhibit only one N atom to coordinate to copper.

As shown in Fig. 7, the plane of Cu-bis(oxazoline) is perpendicular to the plane of O1-C1-C2-C3-O2 in IN3-a, whereas, those planes in IN3-b are almost horizontal. It lead to the energy of IN3-b being higher than IN3-a by about 14.8 kJ $mol^{-1}$ (See Fig. 8).

Starting from IN3, two transition states of TS2-a and TS2-b are found to be responsible for the N-C bond form to give IN4. As shown in Fig. 7, Cu-N3-N4-C2-C3-O2 forms a six-membered ring (the electronic density of RCP for TS2-b is 0.013) in TS2. In an effort to gain some insights into the origin of the steroselectivies observed, we examined the calculated TS2 structure. In TS2-a and TS2-b, Cu-N3 distance is 1.968 Å and 1.949 Å, and Cu-O1 distance is very far, indicate a strong coordination between Cu with N3, and a cleavage of bond between Cu with O1. The configuration of TS2 show a four-coordination character, which is in accord with the characteristic of d9 copper(II) center that favor a square-planar coordination geometry. The N3-N4 bond lengths are 1.296 Å and 1.299 Å in TS2-a and TS2-b, respectively, which is longer than IN3-a and IN3-b (1.233Å and 1.242Å, respectively). It indicates the N=N π-bond change to N-N σ-bond. The cleavage of the N=N π-bond is also confirmed by NBO analysis. The Wiberg bond indexes are lower than those in IN3 (1.43 in TS2-a and 1.41 in TS2-b), the $\epsilon_{BCP}$ of N-N bond (0.13 in IN3-a and IN3-b, 0.11 in TS2-a and 0.10 in TS2-b) are lower than those in IN3, and the Laplacian $\left(\nabla^2_{\rho(r)}\right)$ (-0.98 in IN3-a and -1.12 in IN3-b, -0.84 in TS2-a and TS2-b) in IN3 is more negative, all of the proofs indicate the N-N in IN3 is a double bond and is σ bond in TS2. The N4-C2 distance in TS2-a and TS2-b are 2.021 Å and 2.004 Å, are shorter than in IN3-a and IN3-b, which indicate they have the tendency to form N-C σ-bond.

As shown in Fig. 7, the configuration of TS2-a and TS2-b is very similar, the main difference between TS2-a and TS2-b is the orientation of the ester group connected with N3. In TS2-a, the ester group is close to the 4-positon substituted H, whereas, the ester group of TS2-b is close to methyl. The more crowed structure of TS2-b lead to it to be less stable than TS2-a (TS2-b is higher 16.2 kJ $mol^{-1}$ than TS2-a in the relative energies). However, the barriers of TS2 in both pathway are similar (45.2 kJ $mol^{-1}$ for TS2-a and 46.6 kJ $mol^{-1}$ for TS2-b).

The reaction model allows us to account for the major enantiomers found in the direct amination catalyzed by copper(II). After the TS2, the C-N bond formation step, the chiral-C center is received. The C-N formation step is chiral-determining step. The Cu-N3 distance in IN4-b is shorter than that in IN4-a (1.930Å and 1.912Å in IN4-a and IN4-b, respectively), indicate a stronger coordination between Cu and N3 in IN4-b. On the other hand, the Cu-O2 distance is 2.237 Å in IN4-b, and 2.407 Å in IN4-a.

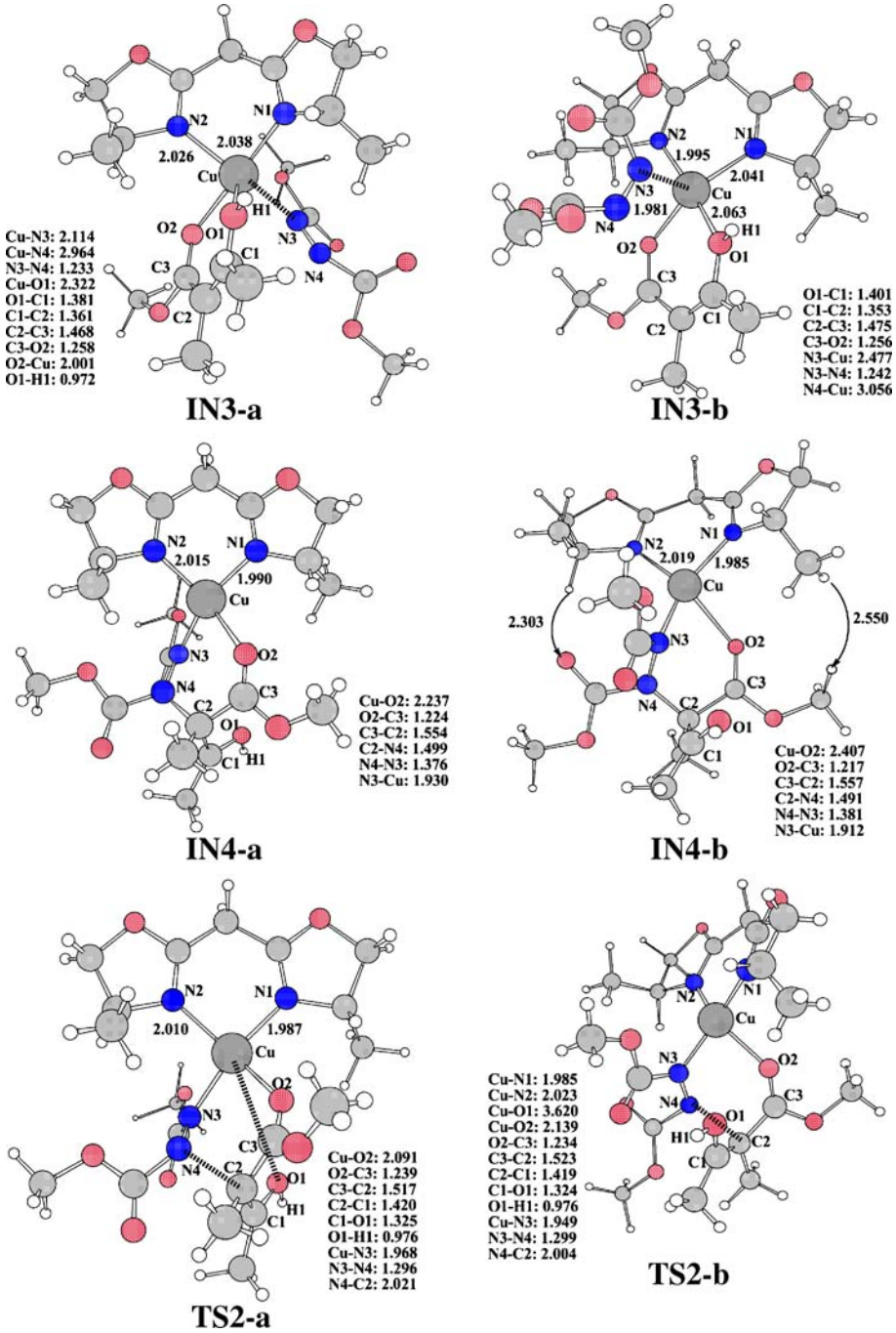


**Fig. 7** B3LYP optimized structures for IN3, TS2 and IN4

Similar to TS2, the crowded structure lead to high energy for IN4-b (the relative Gibbs free energy is -9.2 kJ $mol^{-1}$ for IN4-a, and 2.1 kJ $mol^{-1}$ for IN4-b).

Intramolecular H migration step

The transition structure corresponding to the H migrate from O1 to N3 are located. Figure 9 shows the structures TS3 and IN5. The two structure of TS3 have a H1-N3-N4-C2-C1-O1 six-membered ring (the electronic density of RCP for TS3-b is 0.022). Related to the Cu-N3 and Cu-O1 distance, there are significant change in IN4 and TS3. The Cu-N3 bond from 1.930 Å in IN4-a to 3.603 Å in TS3-a and from 1.912 Å in IN4-b to 3.449 Å in TS3-b. The Cu-N3 bonds are lengthened, it indicate N3 atom no longer coordinate with Cu center. In addition, the interaction between Cu center and O1 atom are strengthened (the Cu-O1 bondlength is 2.048 Å in TS3-a and 2.068 Å in TS3-b, respectively). Therefore, form IN4 to TS3 has a ligand exchange, the coordinated N3 atom eliminated and O1

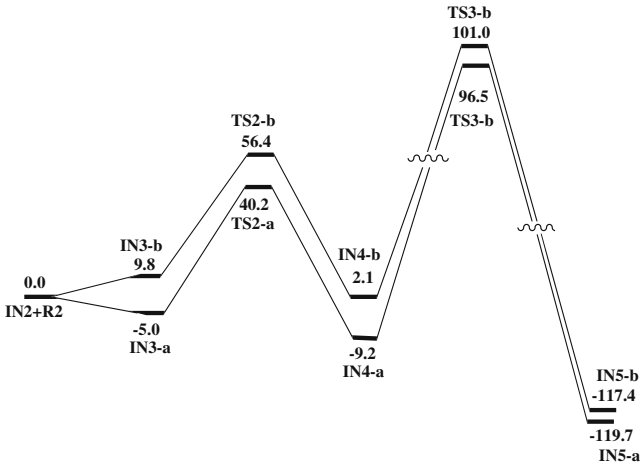


**Fig. 8** Energy profile calculated for the C-N formation and hydrogen migration step for pathway A and pathway B. The relative energies are given in kJ mol$^{-1}$

coordinate to Cu again. The bond of Cu-N3 is strong in IN4, the scission of Cu-N3 lead to a high barrier for TS3, as shown in Fig. 8.

The O1-H1 and H1-N3 distance in TS3-a is 1.402 Å and 1.411 Å, which is 1.420 Å and 1.385 Å in TS3-b. The C1-O1 distance is 1.293 Å and 1.288 Å in TS3-a and TS3-b, respectively, which is shorter than in IN4-a and IN4-b, indicate a hydroxyl bond weakened and a carbonyl bond formed.

The calculated energy barriers for TS3-a and TS3-b are 105.7 and 98.9 kJ mol$^{-1}$, relatively. The relative Gibbs free energies of IN4-a and IN4-b is -9.2 kJ mol$^{-1}$ and 2.1 kJ mol$^{-1}$, respectively, it indicates IN4-a and TS3-a are more stable, which is attributed to the more crewed geometry of IN4-b, there are clear steric between the methoxyl oxygen atom and hydrogen atom of the bis (oxazoline) ligand (2.303 Å) and between the methyl hydrogen atom and one

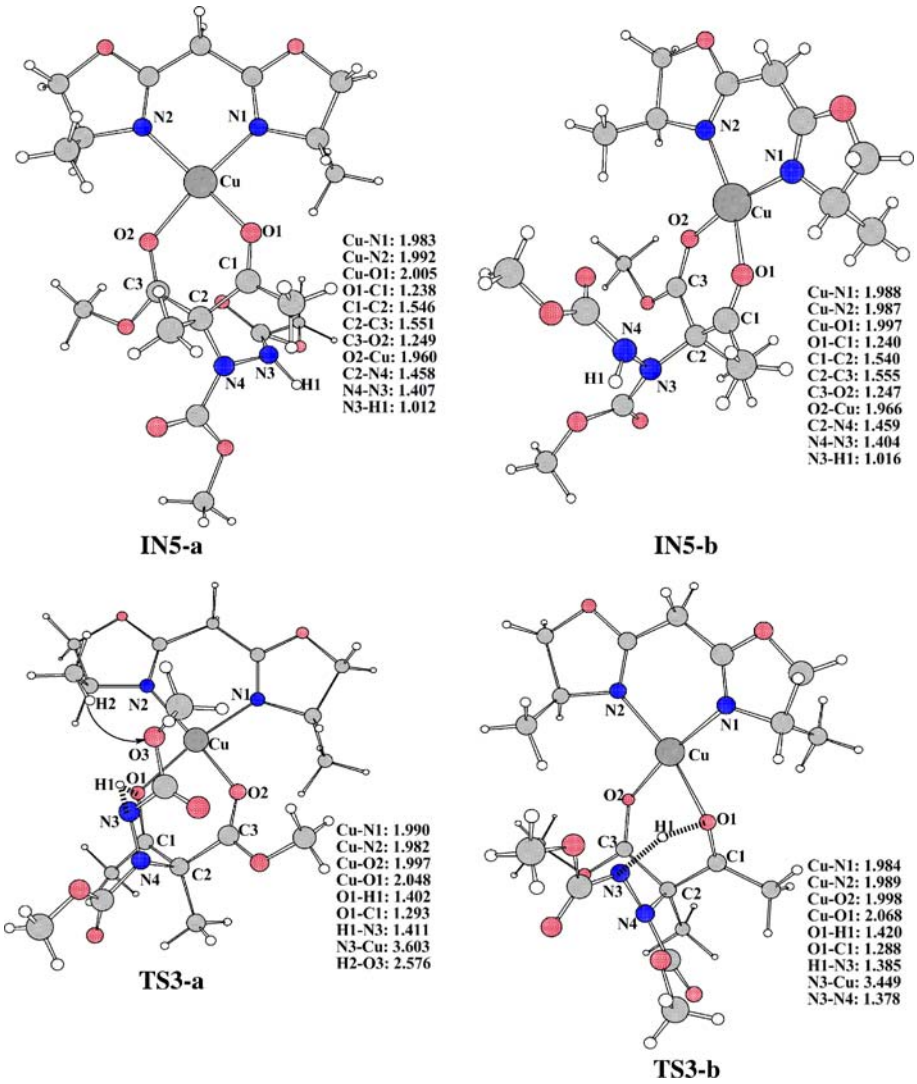


**Fig. 9** B3LYP optimized structures for TS3 and IN5

of hydrogen atoms of the bis(oxazoline) ligand(2.550 Å), just like TS2-b and IN3-b. Nevertheless, after a ligand exchange in TS3, the geometry of TS3-a becomes more crowded, as shown in Fig. 9, the distance of H2 and O3 is 2.576 Å. From the energy viewpoint, the difference between TS3-a and TS3-b is 4.5 kJ $mol^{-1}$, which is less than in IN3, IN4, and TS2 (14.8, 16.2, and 11.3 kJ $mol^{-1}$, respectively).

Inspecting the energy barrier of the entire catalytic process, the highest barriers of TS3 indicate the intramolecular hydrogen migration is the rate-determination step and pathway B is more favorable than pathway A. It is in accord with the experimental result.

After the hydrogen migrate step, a complex (IN5) is formed, in which the α-amino acid product coordinate to the Cu center. The calculated Cu-O1 distance in IN5-a and IN5-b is 2.005 Å, and 1.997 Å. The Cu-O2 distance in IN5-b and IN5-b is 1.960 Å and 1.966 Å, which is similar to the bond length in IN2. It can be seen from Fig. 9, the structure of IN5-a and IN5-b is similar.

This is in agreement with the calculated Gibbs free energy of IN5-a and IN5-b (-119.7 kJ $mol^{-1}$ and -117.4 kJ $mol^{-1}$, respectively). The initial complex Cat is regenerated from this intermediate in order to close the catalytic cycle.

After analysis of each step of the direct amination reaction, a conclusion reached here is that the reaction mechanism shown in Scheme 2 is very feasible. Meanwhile, the downhill potential energy surface (Figs. 3 and 8) discloses that the reaction is irreversible and the overall process is largely favorable from a thermodynamic viewpoint. As demonstrated, the energy barrier is lower for TS3-b than that for TS3-a. Therefore, pathway B is more favorable than pathway A, the mainly chiral product generated along pathway B is (R)-geometry ester which is in agreement with the experiments.

### Solvent effect

The direct amination reaction was carried out in polar solvent; as the solvent can change both gas phase activation energy and stereoselectivity, their effects were explored. The inclusion of solvent effects, such as $CH_2Cl_2$, produces a larger stabilization of the anti enamine than the syn one. The Gibbs free energies and solvation energies of all structures are shown in Table 1. As a consequence, IN3 and IN4 are more stable than in the gas phase. The energy barrier for the chiral-control (TS2) and rate-determining step (TS3) along the more favorable reactive channel (pathway B) decrease to 22.6 and 80.7 kJ $mol^{-1}$, whereas, the rate-determining step barrier for pathway A is increased to 113.5 kJ $mol^{-1}$ (see Fig. 10). These energetic results are in reasonable agreement with experiments, where (R)-configuration product is isolated in 99% ee.

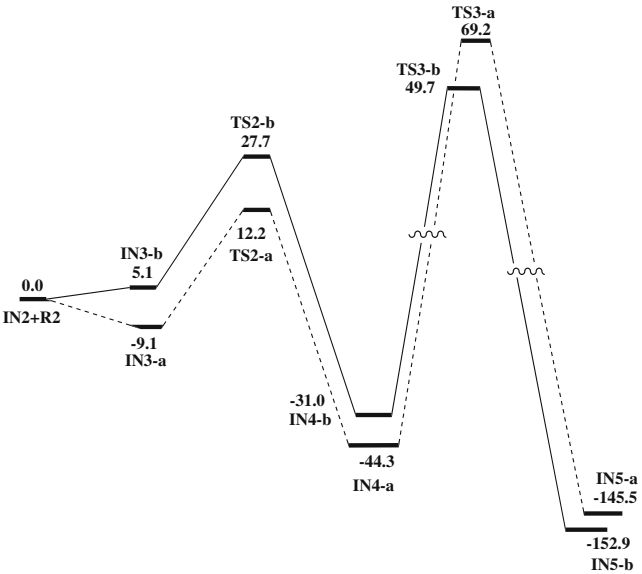


**Fig. 10** Energy profile calculated for the C-N formation and hydrogen migration step for pathway A and pathway B in CH2Cl2 phase. The relative energies are given in kJ $mol^{-1}$

## Conclusions

DFT calculations allow us to propose a reaction mechanism for the direct amination of β-keto esters catalyzed by copper (II)-bisoxazoline (BOX). Under the reaction conditions the catalyst is in coordination with R1–3 in the first, and this step is found to be fast, exothermic, and irreversible. We also considered R1–1 or R1–2 coordinates to the catalyst, followed by 1,3 hydrogen shift to form Cu-enol complex, but the high barriers of hydrogen shift make this channel unfavorable. The azo dicarboxylate also attack chiral Cu(II) catalyst. The N-C bond forming step is the chirality-control step, and give chiral C center. Then, intramolecular hydrogen migration generates a catalyst-product complex, which can finally yield product and the high barrier indicates it is the rate-ditermining step for the entire catalytic cycle. The overall catalytic cycle is highly exergonic. The results of the DFT calculations are in agreement with the experimentaly observed enantioselectives. Careful examination of the optimized geometries of the TS allowed an enantiodifferentiation to be proposed on the basis of the intermolecular steric interaction between the Cat and reactants.

In summary, a thorough examination of the free energy surface of the model reaction studies has allowed the elucidation of the key steps in the mechanism of copper-catalyzed direct amination reactions. This information provides new insights into the origin of the steroselectivities observed, which should allow the design of more efficient catalytic systems.

## References


1. Williams RM (1989) Synthesis of optically active a-amino acids. Pergamon, Oxford
2. Williams RM, Hendrix JA (1992) Chem Rev 92:889–917
3. Arend M (1999) Angew Chem 111:3047–3049; (1999) Angew Chem Int Ed 38:2873–2874
4. Yet L (2001) Angew Chem 113:900–902
5. Duthaler RO (1994) Tetrahedron 50:1539–1650
6. Bergmeier SC (2000) Tetrahedron 56:2561–2576
7. Sigman MS, Jacobsen EN (1998) J Am Chem Soc 120:5315–5316
8. Sigman MS, Vachal P, Jacobsen EN (2000) Angew Chem 112:1336–1338; (2000) Angew Chem Int Ed 39:1279–1281
9. Sigman MS, Jacobsen EN (1998) J Am Chem Soc 120:4901–4902
10. Krueger CA, Kuntz KW, Dzierba CD, Wirschun WG, Gleason JD, Snapper ML, Hoveyda AH (1999) J Am Chem Soc 121:4284–4285
11. Takamura M, Hamashima Y, Usuda H, Kanai M, Shibasaki M (2000) Angew Chem 112:1716–1718; (2000) Angew Chem Int Ed 39:1650–1652
12. Corey EJ, Grogan MJ (1999) Org Lett 1:157–160
13. Ishitani H, Komiyama S, Kobayashi S (1998) Angew Chem 110:3369–3372; (1998) Angew Chem Int Ed 37:3186–3188
14. Ishitani H, Komiyama S, Hasegawa Y, Kobayashi S (2000) J Am Chem Soc 122:762–766
15. Juhl K, Jrogensen KA (2002) J Am Chem Soc 124:2420–2421
16. Marigo M, Juhl K, Jrogensen KA (2003) Angew Chem Int Ed 42:1367–1369
17. Ghosh AK, Mathivanan P, Cappiello J (1998) Tetrahedron: Asymmetry 9:1–45
18. Jørgensen KA, Johannsen M, Yao S, Audrain H, Thurhauge J (1999) Acc Chem Res 32:605–613
19. Evans DA, Rovis T, Johnson JS (1999) Pure Appl Chem Res 71:1407–1415
20. Lee C, Yang W, Parr RG (1988) Phys Rev B 37:785–789
21. Becke AD (1993) J Chem Phys 98:5648–5652
22. Gonzalez C, Schlegel HB (1989) J Chem Phys 90:2154–2159
23. Hay PJ, Wadt WR (1985) J Chem Phys 82:270–283
24. Wadt WR, Hay PJ (1985) J Chem Phys 82:284–298
25. Hay PJ, Wadt WR (1985) J Chem Phys 82:299–310
26. Hariharan PJ, Pople JA (1973) Theor Chim Acta 28:213–222
27. Frisch MJ, Trucks GW, Schlegel HB, Scuseria GE, Robb MA, Cheeseman JR, Montgomery JA, Vreven T Jr, Kudin KN, Burant JC, Millam JM, Iyengar SS, Tomasi J, Barone V, Mennucci B, Cossi M, Scalmani G, Rega N, Petersson GA, Nakatsuji H, Hada M, Ehara M, Toyota K, Fukuda R, Hasegawa J, Ishida M, Nakajima T, Honda Y, Kitao O, Nakai H, Klene M, Li X, Knox JE, Hratchian HP, Cross JB, Adamo C, Jaramillo J, Gomperts R, Stratmann RE, Yazyev O, Austin AJ, Cammi R, Pomelli C, Ochterski JW, Ayala PY, Morokuma K, Voth GA, Salvador P, Dannenberg JJ, Zakrzewski VG, Dapprich S, Daniels AD, Strain MC, Farkas O, Malick DK, Rabuck AD, Raghavachari K, Foresman JB, Ortiz JV, Cui Q, Baboul AG, Clifford S, Cioslowski J, Stefanov BB, Liu G, Liashenko A, Piskorz P, Komaromi I, Martin RL, Fox DJ, Keith T, Al-Laham MA, Peng CY, Nanayakkara A, Challacombe M, Gill PMW, Johnson B, Chen W, Wong MW, Gonzalez C, Pople JA (2003) Gaussian 03, Revision B.03. Gaussian Inc, Pittsburgh PA
28. Glendening ED, Reed AE, Carpenter JE, Weinhold F NBO version 3.1
29. Carpenter JE, Weinhold F (1988) J Mol Struct (Theochem) 169: 41–62
30. Charpenter JE (1987) Dissertation, Univ Wisconsin, Madison, WI
31. Foster JP, Weinhold F (1980) J Am Chem Soc 102:7211–7218
32. Reed AE, Weinhold F (1983) J Chem Phys 78:4066–4073
33. Reed AE, Weinhold F (1985) J Chem Phys 83:1736–1740
34. Reed AE, Weinstock RB, Weinhold F (1985) J Chem Phys 83:735–746
35. Reed AE, Curtiss LA, Weinhold F (1988) Chem Rev 88:899–926
36. Weinhold F, Carpenter JE (1988) Plenum p 227–236
37. Biegler-König F, Schönbohm J, Derdau R, Bayles D, Bader RFW (2000) AIM 2000 version 1
38. Miertus S, Tomasi J (1982) Chem Phys 65:239–245
39. Ehlers AW, Böhme M, Dapprich S, Gobbi A, Höllwarth A, Könler VJKF, Stegmann R, Veldkamp A, Frenking GA (1993) Chem Phy Let 208:237–240
40. Gorelsky SI, Lever ABP (2001) J Organomet Chem 635:187–196
41. Gorelsky SI, AOMix: Program for Molecular Orbital Analysis; York University: Toronto, Canada, 1997; http://www.sf-chem.net/
42. Gorelsky SI, Ghosh S, Solomon EI (2006) J Am Chem Soc 128:278–290
43. Wiberg KB (1968) Tetrahedron 24:1083–1096
44. El-Dissouky A, Refaat LS (1987) Inorg Chem Acta 87:213–222
45. Fraile JM, Garcia JI, Martinez-Merino V, Mayoral JA, Salvatella L (2001) J Am Chem 123:7616–7625
46. Evans DA, Miller SJ, lectka T, von Matt P (1999) J Am Chem Soc 121:7559–7573
47. Audrain H, Thorhauge J, Hazell RG, Jørgensen KA (2000) J Org Chem 65:4487–4497